


## ARTICLE

# Toward the definition of equivalent damage parameters for the assessment of corroded RC structures

Elena Casprini<sup>1</sup>  | Chiara Passoni<sup>1</sup>  | Alessandra Marini<sup>1</sup>  | Gianni Bartoli<sup>2</sup> 

<sup>1</sup>Department of Engineering and Applied Sciences, University of Bergamo, Dalmine, Italy

<sup>2</sup>Department of Civil and Environmental Engineering, University of Florence, Firenze, Italy

## Correspondence

Elena Casprini, Department of Engineering and Applied Sciences, University of Bergamo, Dalmine, BG, 24044, Italy.

Email: [elena.casprini@unibg.it](mailto:elena.casprini@unibg.it)

## Abstract

The effects of reinforcement corrosion need to be included in the assessment of existing Reinforced Concrete structures for a reliable evaluation of the structural performances over time and a correct choice of the renovation strategy. The DEMSA protocol proposes straightforward tools available to professional engineers, enabling the calibration of equivalent damage parameters able to describe corrosion effects starting from environmental easy-measurable conditions. Guidance to implement the equivalent damage parameters describing corrosion effects at a sectional level in the structural analyses is provided. Then, a simplified approach to model the corrosion attack distribution along the bar length is proposed. Finally, nonlinear static analyses are carried out on reference RC frames subjected to different corrosion patterns by adopting fiber modeling technique, to show how the equivalent damage parameters allow detecting the impact of corrosion effects on the structural performances, in terms of internal actions distribution, reduction of stiffness, strength, and ductility.

## KEYWORDS

corrosion attack distribution, corrosion effects, equivalent damage parameters, fiber models, RC structures, structural assessment

## 1 | THE DEMSA PROTOCOL FOR RC STRUCTURES

Corrosion of reinforcement may involve any RC structure under specific environmental and aggressiveness conditions, strongly affecting its structural behavior. Despite that, in the current practice, corrosion effects are seldom

included in the structural diagnosis and assessment process, unless corrosion signs are clearly manifest on concrete surface; this may lead to an ineffective structural modeling, and consequently, to unreliable predictions of the structural performance. The lack of awareness of possible consequences of deterioration processes in structural applications is in contrast with the deep knowledge available in the literature. Though corrosion process and its consequences on steel and surrounding concrete material are well known in the field of electrochemistry and material engineering<sup>1,2</sup>; structural engineers recently developed analytical models to evaluate the residual

Discussion on this paper must be submitted within two months of the print publication. The discussion will then be published in print, along with the authors' closure, if any, approximately nine months after the print publication.

This is an open access article under the terms of the [Creative Commons Attribution-NonCommercial-NoDerivs](https://creativecommons.org/licenses/by-nc-nd/4.0/) License, which permits use and distribution in any medium, provided the original work is properly cited, the use is non-commercial and no modifications or adaptations are made.

© 2022 The Authors. *Structural Concrete* published by John Wiley & Sons Ltd on behalf of International Federation for Structural Concrete.

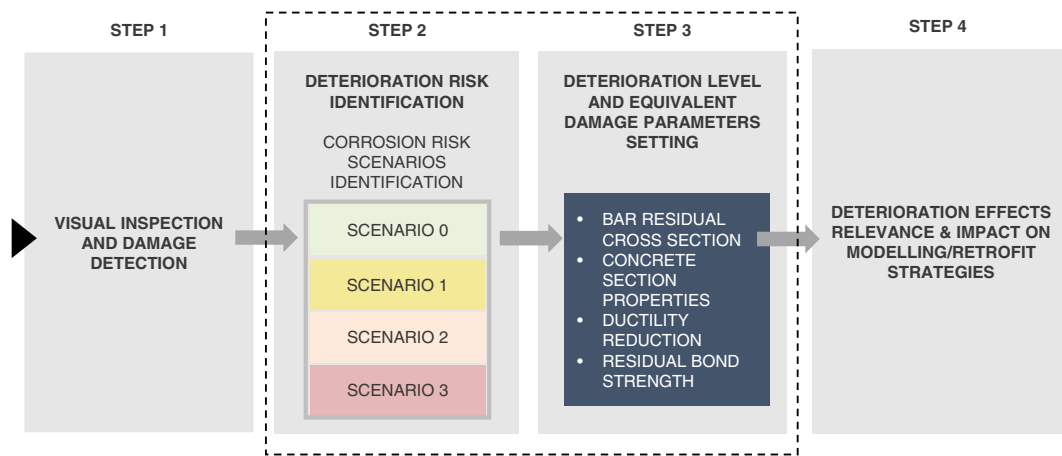


**FIGURE 1** Steps of the DEMSA protocol: step (1) visual inspection; step (2) definition of the deterioration risk; step (3) estimation of the deterioration level; step (4) definition of the deterioration effect relevance and impacts on the preliminary selection of the renovation strategy (adapted from Casprini et al.<sup>6</sup>)

strength of corroded RC members<sup>3</sup> and validated them against experimental data. However, for the practical applications of assessment of existing RC structures, important issues need to be addressed. The existing analytical and numerical models would require the definition of the corrosion level as input data, which is highly variable and difficult to determine on site; also, the level of accuracy at which phenomena are investigated at material level is often not applicable at the scale of the structure. Therefore, from the designer point of view, the applicability of the available knowledge into the diagnosis and assessment process may be limited due to the lack of a shared simplified multidisciplinary approach dealing with all the sectorial fields involved in the problem.<sup>6</sup> A great effort is being made recently to integrate such knowledge in the current practice, involving both researchers and practitioner engineers.<sup>4,5</sup>

In this context, the recently proposed DEMSA Protocol<sup>6</sup> (Deterioration Effect Modeling for Structural Assessment) provides a step-by-step procedure guiding the engineer from building inspection to structural evaluation and selection of the best renovation strategy by including corrosion effects. In the Protocol, validated aspects from the literature are collected, and new tools allowing interaction among the different levels of the assessment process are integrated. The main advancements introduced in the protocol with respect to the current knowledge consist in: (i) ordinating and systematizing the already validated diagnosis techniques to identify the possible risk of corrosion (classified in Corrosion Risk Scenarios; step 1–2); (ii) introducing a straightforward method to relate the environmental and aggressiveness conditions measured in-field with simple equivalent damage parameters (EDP; step 3);

(iii) allowing the evaluation of deterioration effects on the structural performances and their impact on the modeling/retrofit strategy (step 4; Figure 1). Such a protocol is conceived as a flexible, simplified framework, tested through its application to several existing structures,<sup>6</sup> in which the designer is guided from the in-situ inspection to the identification of a Corrosion Risk Scenario, gaining awareness of the relevance of the corrosion effects on the structural performance, up to the calibration of an equivalent defect modeling such effects in the structural analysis. While the overall roadmap is clearly defined as a series of consecutive actions, with the necessary input data and output information clearly stated for each step, the specific formulations adopted can be easily substituted or updated in relation to the type of structure under investigation, or to account for future research findings. Also, further research is needed in each field of expertise, to refine the available formulations and better calibrate the characteristics of the corrosion attack. In this paper, the focus is made on the definition, calibration, and application of the equivalent damage parameters as a tool for accounting for corrosion in the structural assessment.

## 2 | EQUIVALENT DAMAGE PARAMETERS

Corrosion damage reduces the stiffness, the strength, and the ductility of RC members.<sup>7</sup> The mechanical behavior of corroded RC members is primarily related to the characteristics of the corrosion attack on the steel bars directly affected by corrosion processes, which are described through the corrosion penetration on the bar

section (determining both the bar residual strength and the properties of cracked concrete) and the attack distribution along the bar length (affecting the residual elongation capacity and bond strength). Some equivalent damage parameters can thus be introduced to simulate possible corrosion attack intensity and patterns at different levels of a multi-scale analysis, from the evaluation of the residual sectional capacity of RC members to the assessment of the global structural behavior.

## 2.1 | Corrosion attack on the element section

As for the sectional capacity of RC beams and columns, corrosion damage can be quantified in a possible reduction of the steel bar cross-section and mechanical properties, and the cracking of the concrete cover surrounding the bars, as corrosion products expand. According to the formulations currently available in the literature,<sup>3,8</sup> these effects can be estimated starting from the average and maximum corrosion attack penetration into the bar cross-section. Such information cannot be easily collected on site, since its direct measurement requires either the disruptive removal of concrete cover in few locations (which cannot be representative of the whole structure), or the application of electrochemical techniques for the estimation of the corrosion rate (i.e., corrosion attack penetration over time, measured in  $\mu\text{m}/\text{year}$ ) which are not reliable for single in-field inspections.<sup>9</sup>

In the DEMSA Protocol, to overcome this issue, the corrosion attack characteristics are related to easy-measurable environmental and aggressiveness conditions, grouped into four categories, labeled as Corrosion Risk Scenarios<sup>6</sup> (CRS). The exposure classes from EN206<sup>10</sup> are considered, although they are re-classified into such new Scenarios having the same expected type and pattern of corrosion. In detail, exposure conditions inhibiting corrosion or leading to corrosion attacks with a negligible corrosion rate (not significant for the structural performance, lower than  $1\text{--}2 \mu\text{m}/\text{year}$ <sup>1</sup>) are included in Scenario 0; Scenario 1 refers to carbonation-induced corrosion in absence of chlorides, which becomes significant only in presence of wet/dry cycles or high relative humidity (R.H.  $>70\%$ ); Scenario 2 to the simultaneous presence of low chloride content ( $0.1\% < \text{Cl}^- < 0.4\%$  with respect to cement weight, that is below chloride threshold for pitting corrosion initiation) and carbonation, which effects cannot be disregarded in existing structures,<sup>1,11</sup> also in moderate humidity condition (R.H.  $> 50\%$ ); and Scenario 3 to chloride-induced corrosion (chloride content in the cementitious matrix  $\text{Cl}^- > 0.4\%$  with respect to cement weight). Also, within

each Scenario, three aggressiveness classes are included (Ordinary, High, Extreme) based on the level of relative humidity (R.H.), concrete quality or chloride content, to better quantify the intensity of the attack.

Based on the classification in Corrosion Risk Scenarios and aggressiveness classes, a representative value of the average corrosion rate  $v_{\text{avg}}$  (i.e., the rate of the average corrosion attack penetration on rebars measured in  $\mu\text{m}/\text{year}$ ) and of the maximum to average attack ratio  $R_p$  (i.e., a ratio between the maximum and average corrosion attack) are tentatively defined in the protocol<sup>6</sup> (Table 1); such preliminary values are derived from literature of corrosion experts<sup>1,12–14</sup> in relation to specific environmental conditions, or measured on corroded bars extracted from existing structures belonging to different Scenarios.<sup>8</sup> Further research is thus needed on this aspect, to collect a wider database of information, which would allow increasing the reliability of these corrosion characteristics. These primary characteristics of the corrosion attack allow for the definition of the equivalent damage parameters by following the procedure synthesized in Figure 2. Once  $v_{\text{avg}}$  and  $R_p$  are chosen, the bar average and minimum residual cross-section may be calculated by defining both the propagation time and the attack model on the bar section.

The propagation time  $T_p$  (herein defined as the time from bar depassivation to the time of the survey, in the case corrosion is active) can be preliminary estimated starting from the measurement of aggressive substances penetration depth in the concrete cover at the time of the survey, as suggested in the CONTECVET manual.<sup>9</sup> Indeed, steel bars are depassivated (unprotected from corrosion attack) when either the carbonation front (leading to a drop in the PH of the pore solution) or a critical chloride threshold (locally destroying the passive protection film) reach the rebar level. A value for the aggressive substances penetration rate  $K$  is estimated in a simplified manner according to the square root formula (Equation 1):

$$K = \frac{d}{\sqrt{t}} = \frac{d\text{CO}_2(d\text{Cl})}{\sqrt{T_a - T_{0,\text{agg}}}} \quad (1)$$

where  $d$  is the depth of penetration in mm and is calculated from the measurement of the carbonation  $d\text{CO}_2$  (or chloride profile  $d\text{Cl}$ ) penetration depth measured on-site; and  $t$  is the time in years, which is the difference between the age of the structure  $T_a$ , calculated as the time frame from construction ( $T_0$ ) to the year of survey ( $T_{\text{survey}}$ ), and the time since the aggressive substance started to penetrate from the concrete edge ( $T_{0,\text{agg}}$ ). The latter usually corresponds with  $T_0$  unless environmental

Attack	Aggressiveness	CRS 1	CRS 2	CRS 3
Average corrosion rate $v_{avg}$ ( $\mu\text{m}/\text{year}$ )	CLASS ordinary		2÷10	10÷50
	CLASS high	2÷10	10÷50	50÷100
	CLASS extreme	10÷50	100÷200	100÷300
Maximum to average attack ratio $R_p$		1÷2	3÷7	4÷10

**TABLE 1** Proposal of representative values of corrosion attack characteristics corresponding to each corrosion risk scenario (CRS) and aggressiveness class

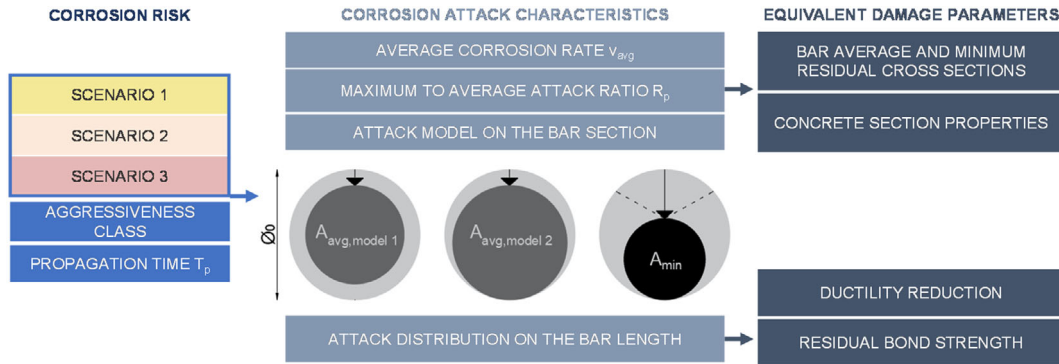


**FIGURE 2** Definition of the equivalent damage parameters to be implemented: In blue the input data related to corrosion risk, in light blue the corrosion attack characteristics selected from the Scenarios, in dark blue the final equivalent damage parameters<sup>6</sup>

aggressiveness conditions may have changed during the structure life.<sup>6</sup> Then, the time necessary for the aggressive substances to reach bars (initiation time  $T_i$ ) is calculated (Equation 2):

$$T_i = \frac{cc^2}{K^2} + T_{0,agg} \quad (2)$$

where  $cc$  is the concrete cover dimension. Finally, the propagation time is obtained as  $T_p = T_a - T_i$ . The average attack can be modeled as symmetric (herein defined as Model 1, Figure 2) or asymmetric (Model 2) as proposed by Andrade<sup>15</sup>; the former, with the attack penetrating from all sides of the bar, may be representative if chlorides are present in the cementitious matrix surrounding the bar, while the latter could be more appropriate if a corrosion attack due to the presence of water in contact with the rebars occurs, mainly coming from one side.

The bar average residual cross-section  $A_{avg}$  is obtained from Equation 3, where  $\phi_0$  is the original bar diameter; the minimum residual cross-section  $A_{min}$  is calculated by assuming that the maximum corrosion attack penetration is equal to the bar diameter reduction (Equation 4), and that the area surrounding the localized attack is neglected for the calculation of the effective minimum residual cross-section.<sup>15</sup> While  $A_{min}$  is connected to the bar residual strength, also  $A_{avg}$  is essential to model the distribution of the corrosion attack along the bar length, as proposed in Section 2.

$$A_{avg,model 1} = \frac{\pi(\phi_0 - 2 \cdot v_{avg} \cdot T_p)^2}{4}$$

$$A_{avg,model 2} = \frac{\pi(\phi_0 - v_{avg} \cdot T_p)^2}{4} \quad (3)$$

$$A_{min} = \frac{\pi(\phi_0 - v_{avg} \cdot R_p \cdot T_p)^2}{4} \quad (4)$$

Not all the researchers agree on the possible relationship between steel-bar mechanical properties deterioration and corrosion. For mild steel plain bars, it has been observed that, if the minimum cross-section is considered, the yield and ultimate stresses of corroded bars do not change significantly with respect to the uncorroded one.<sup>16</sup> In contrast, mechanical properties may be reduced in bars produced nowadays, often obtained through thermo-mechanical processes or addition of micro-binders, since the outer layer of the bar, which is mainly affected by corrosion, may be characterized by a higher hardness and strength with respect to the internal core; in this case, a reduced steel strength can be calculated according to formulations proposed in the literature.<sup>17</sup> When considering existing RC structures, especially from the '50'-70, where plain bars are often found, yielding and ultimate stresses may be assumed to be equal to those of the virgin material, as also assumed in the future version of the Model Code 2020.<sup>18</sup>

Addressing concrete material properties, a reduced compressive strength is calculated for cracked concrete cover, dependent on the corrosion attack penetration, as proposed in Coronelli & Gambarova<sup>19</sup> through Equation 5, where  $k$  is a coefficient related to bar roughness and diameter (assumed as 0.1 for medium-ribbed bars);  $\varepsilon_{c0}$  is the strain associated with the maximum compressive stress  $f_c$  (uncracked concrete) and  $\varepsilon_1$  the average tensile strain in the cracked concrete (Equation 6). In this case,  $b_0$  is the section width in the uncracked stage and  $b_f$  the section width increased by corrosion cracking, approximated as in Equation 7, where  $n_{\text{bars}}$  is the number of bars in the top layer (compression zone) and  $w_{cr}$  the total crack width for a corrosion level  $p$  (penetration of the corrosion attack), which is evaluated by following Molina et al.<sup>20</sup> as reported in Equation 8;  $\nu_{rs}$  is the ratio of volumetric expansion of the oxides with respect to the virgin material (assumed equal to 2) and  $u_{i,\text{corr}}$  the opening of each corrosion crack.

$$f_c^* = \frac{f_c}{1 + k \cdot \varepsilon_1 / \varepsilon_{c0}} \quad (5)$$

$$\varepsilon_1 = (b_f - b_0) / b_0 \quad (6)$$

$$b_f - b_0 = n_{\text{bars}} \cdot w_{cr} \quad (7)$$

$$w_{cr} = \sum_i u_{i,\text{corr}} = 2\pi(\nu_{rs} - 1)p \quad (8)$$

In the protocol, the formulations required to calibrate the equivalent damage parameters were selected among those currently adopted by researchers, proposed as reference in the literature.<sup>6</sup> However, it is worth emphasizing that the reliability of the adopted formulations or input data does not compromise the validity of the proposed procedure, since each formula can be easily updated/substituted to comply with future research findings or as a result of different design choices.

## 2.2 | Corrosion attack distribution along the element length

As for the assessment of the whole element structural behavior, the reduction in ductility should also be considered. To date, the most adopted model<sup>19</sup> considers an equivalent reduction of the bar ultimate strain as dependent on the bar minimum residual cross-section (due to pitting attack). However, recent studies<sup>8,18,21</sup> showed that the spatial distribution of the maximum attack may be the most influencing factor in the bar

elongation capacity reduction. In real applications, the distribution of the corrosion attack along the bar length cannot be extensively known. Therefore, a simplified method to relate such distribution with a simplified attack is proposed herein: first, an analytical model providing the ductility reduction of a bar with a simplified corrosion attack distribution (characterized by a single defect of length  $L_c$  where the maximum attack occur) is derived, then, a proposal to relate natural uneven corrosion attack distribution to such simplified one is presented starting from corrosion patterns measured on few bars extracted from existing structures. More data on corrosion patterns found in naturally corroded bars are necessary to introduce such a single equivalent defect (with length  $L_c$  and bar cross section  $A_{\text{min}}$ ) as a corrosion attack characteristic provided along with the Corrosion Risk Scenarios.

### 2.2.1 | Analytical model for the bar elongation capacity reduction

The problem can be analytically investigated by assuming an ideal bilinear stress-strain constitutive relationship with hardening for the steel (Figure 3a). The mechanical properties of the virgin material are the yielding stress  $f_y$ , the maximum stress  $f_u$ , the elastic modulus  $E_s$ , the strain at yielding  $\varepsilon_y = f_y/E_s$ , the ultimate strain  $\varepsilon_u$ , and the reduced elastic modulus  $E_{s,r} = (f_u - f_y)/(\varepsilon_u - \varepsilon_y)$ . If such properties are considered not to change due to corrosion, the apparent reduction in ductility is solely due to the reduction of the total elongation capacity of the bar, which is included in the model by considering an equivalent ultimate strain  $\bar{\varepsilon}_{\text{eq},u}$  rather than  $\varepsilon_u$ .

Given a generic residual cross-section profile  $A(x)$ , being  $x$  a variable along the bar longitudinal axis, the tensile stress  $\sigma(x)$  in each section of the bar is given by the ratio between the force  $F(x)$  in that section and the cross-section  $A(x)$ ; the strain in each section  $\varepsilon(x)$  can be then calculated by evaluating whether the stress in that section has reached the yielding stress  $f_y$  or not. For this reason, different levels of deformation (elastic or plastic) are present in the different sections of the bar, in the case of uneven distribution of the corrosion attack (Equation 9).

$$\varepsilon(x) = \begin{cases} \sigma(x)/E_s & \sigma(x) < f_y \\ \varepsilon_y + (\sigma(x) - f_y)/E_{s,r} & f_y \leq \sigma(x) \leq f_u \end{cases} \quad (9)$$

The maximum elongation of the bar at failure  $\Delta l_u$  is obtained by integrating the strain along the bar at failure. The ratio of such maximum elongation over the initial



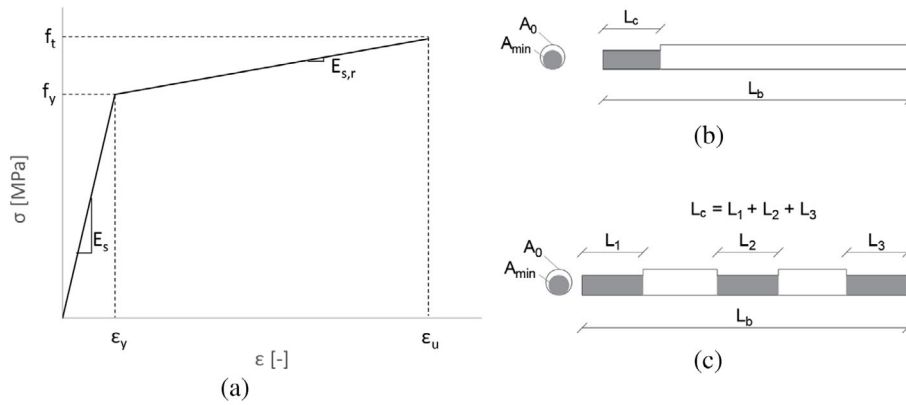


FIGURE 3 Idealized stress–strain constitutive law for steel material (a); simplified corrosion patterns for bars of length  $L_b$  and uniform cross-section  $A_0$  with a single defect (b) or multiple defect (c) for a total length  $L_c$  associated with a cross-section  $A_{\min}$

bar length  $L_b$  provides the equivalent average ultimate strain  $\bar{\epsilon}_{\text{eq},u}$  (Equation 10):

$$\bar{\epsilon}_{\text{eq},u} = \frac{\Delta l_u}{L_b} = \frac{1}{L_b} \int_0^{L_b} \epsilon(x) dx \leq \epsilon_u \quad (10)$$

In the generic case of a non-uniform force distribution  $F(x)$  along the bar length, the solution to the problem requires the identification of both the section in which failure occurs and the maximum force reached  $F_u$ . Indeed, in this case, the location of the section in which the maximum stress  $f_u$  is expected depends on both the cross-section  $A(x)$  and the axial force  $F(x)$  distributions. Once the failure force is determined, the stress in each section, and consequently the strain, can be calculated, thus deriving the maximum elongation.

In the specific configuration of a bar subjected to a constant tensile axial force distribution along its length  $F(x) = F$ , the tensile stress  $\sigma(x)$  is only a function of the cross-section distribution, and the minimum cross section  $A_{\min} = \min(A(x))$  governs the bar behavior in terms of strength. At yielding and at failure, the force is  $F_y = A_{\min} f_y$  and  $F_u = A_{\min} f_u$ , respectively; consequently,  $\bar{\epsilon}_{\text{eq},u}$  is obtained. Under the hypothesis of constant distribution of tensile axial force, a simplified formulation for the equivalent ductility reduction of a bar with length  $L_b$  and a single defect of length  $L_c$  (corroded length) is derived. In the defect, a residual cross-section  $A_{\min}$  is assumed (Figure 3b); such a representation is also valid if more defects are present, as long as the maximum attack is equal in all the defects; in this case, the length  $L_c$  is given by the sum of the defect lengths (Figure 3c). The cross-section  $A_0$  in the rest of the bar can be either the original uncorroded section or the average residual section. The length associated with  $A_0$  is called  $L_0 = L_b - L_c$ .

In this configuration, the expression of  $\bar{\epsilon}_{\text{eq},u}/\epsilon_u$  is obtained as dependent on two dimensionless parameters, namely  $L_c/L_b$  and  $A_{\min}/A_0$  (Equation 11), where  $\epsilon_0$  is a

function of the tensile stress in the section  $A_0$  as expressed in Equation 12.

$$\frac{\bar{\epsilon}_{\text{eq},u}}{\epsilon_u} = \frac{\Delta l_u}{L_b \epsilon_u} = \frac{\epsilon_u L_c + \epsilon_0 L_0}{L_b \epsilon_u} = \frac{L_c}{L_b} + \frac{L_0}{L_b} \frac{\epsilon_0}{\epsilon_u} = \frac{L_c}{L_b} + \left(1 - \frac{L_c}{L_b}\right) \frac{\epsilon_0}{\epsilon_u} \quad (11)$$

$$\epsilon_0 = \begin{cases} f_0/E_s & f_0 < f_y \\ \epsilon_y + (f_0 - f_y)/E_{s,r} & f_y \leq f_0 \leq f_u \end{cases} \quad (12)$$

The stress  $f_0$  in the section  $A_0$  at bar failure, is calculated according to Equation 13, being the section of interest known.

$$A_0 \cdot f_0 = A_{\min} \cdot f_u \rightarrow f_0 = f_u \cdot \frac{A_{\min}}{A_0} \quad (13)$$

Therefore, two different expressions of  $\bar{\epsilon}_{\text{eq},u}/\epsilon_u$  are derived, depending on whether the yielding stress is reached or not in the section  $A_0$  (Equation 14). Such expressions represent the residual ductility in the corroded bar with respect to the original one. In the second case, the term  $\epsilon_y$  may even be disregarded, being at least an order of magnitude lower than the other term in brackets.

$$\frac{\bar{\epsilon}_{\text{eq},u}}{\epsilon_u} = \begin{cases} \frac{L_c}{L_b} + \left(1 - \frac{L_c}{L_b}\right) \frac{f_u A_{\min}}{E_s A_0} \frac{1}{\epsilon_u} & f_0 < f_y \\ \frac{L_c}{L_b} + \left(1 - \frac{L_c}{L_b}\right) \left( \epsilon_y + \frac{f_u A_{\min} - f_y}{E_{s,r}} \right) & f_y \leq f_0 \leq f_u \end{cases} \quad (14)$$

Such expression allows performing some considerations: if  $L_c = L_b$  (uncorroded bar or uniform corrosion

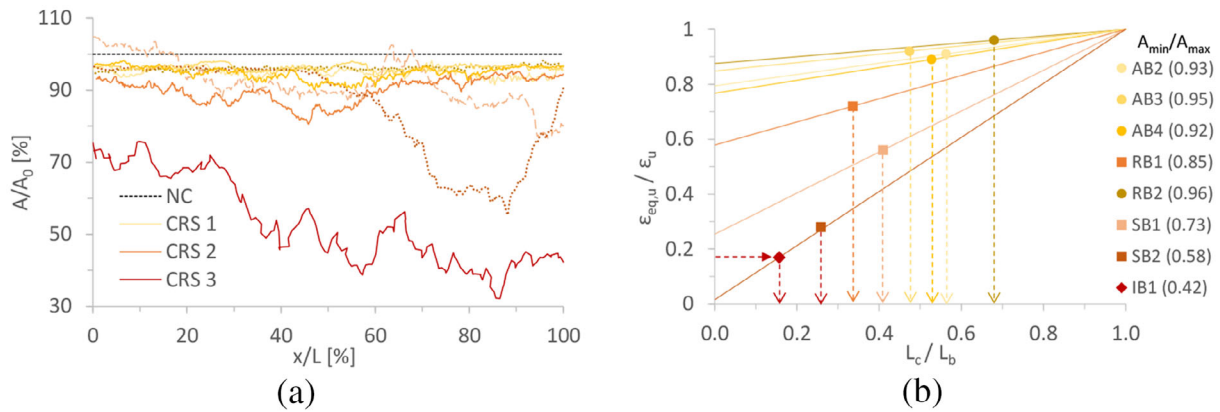


**FIGURE 4** Residual cross-section profile along the bar length (a) and equivalent defect length (b) of corroded bars from different corrosion risk Scenarios (from Casprini et al, 2022<sup>22</sup>)

pattern), there is no reduction in ductility, since it provides  $\bar{\epsilon}_{eq,u}/\epsilon_u = 1$ ; also, being the second term in both the expressions in Equation 14 always non negative,  $L_c/L_b$  (which is associated with the elongation reached in the defect) can be always assumed as a lower-bound value of the expression  $\bar{\epsilon}_{eq,u}/\epsilon_u$ . Moreover, when yielding is not reached in the section  $A_0$  ( $f_0 < f_y$ ), values of  $\bar{\epsilon}_{eq,u}/\epsilon_u$  are very close to  $L_c/L_b$ , since the second term becomes almost negligible; this means that, in these specific cases, the reduction in ductility is only dependent on the length of the defect with respect to the bar and it cannot be described solely by the minimum cross-section.

### 2.2.2 | Relation between natural corrosion patterns and simplified ones

The proposed analytical model allows calculating the residual elongation capacity of a bar with an uneven corrosion pattern (Equations 9–10) and of a bar with a single defect of length  $L_c$  with section  $A_{min}$  (Equation 14), when subjected to a constant distribution of the tensile axial force. The aim of the proposed approach is to relate natural corrosion patterns to simplified attack distributions to be included in the structural models by equalling the calculated residual elongation capacities with the above mentioned equations; this would provide the definition of an equivalent defect length along with the corrosion attack characteristics of each Scenario. To define such a parameter, the geometrical distribution of the corrosion attack needs to be measured on a large number of naturally corroded bars for each Scenario and aggressiveness class. As a proof of the concept, the residual cross-section distribution measured in 8 bars extracted from 4 corroded structures in different Scenarios was considered.<sup>8</sup>The residual cross-sections of the bars were measured through tomographic scans (a summary of the results is

reported in Figure 4a). The maximum force at failure can be calculated by assuming the ideal bilinear stress–strain relationship described in Figure 3a ( $E_s = 210,000$  MPa,  $E_{s,r} = 2100$  MPa,  $f_y = 360$  MPa,  $f_u = 566$  MPa,  $\epsilon_y = 0.0017$ ,  $\epsilon_u = 0.1$ ); therefore, values of the stress and strain in each section at failure are obtained (according to Equation 9). The integral of the strains along the bar divided by the bar length provides  $\bar{\epsilon}_{eq,u}$  (Equation 10), which is then compared with the assumed ultimate strain of the reference material;  $A_{min}$  and  $A_0$  (original cross-section) are known for the considered bars. Using the values of  $\bar{\epsilon}_{eq,u}/\epsilon_u$  and  $A_{min}/A_{max}$  for each bar, an equivalent defect length over the bar length  $L_c/L_b$  is estimated from the plot in Figure 4b (which is the graphical representation of Equation 14). Bars associated with Corrosion Risk Scenarios 1, 2, 3 are shown with yellow circles, orange squares and red rhombus, respectively. It is observed that, for the examined bar, in Scenario 1 (AB2, AB3, AB4, RB2), the equivalent ratio  $L_c/L_b$  is always higher than 45% with an equivalent elongation capacity reduction ranging between 89% and 96% with respect to the original material. As for bars associated with Scenario 2 (RB1, SB1, SB2),  $L_c/L_b$  ranges between 25%÷40% and  $\bar{\epsilon}_{eq,u}/\epsilon_u$  between 30% and 70%. For the unique bar in Scenario 3 (IB1),  $L_c/L_b$  is equal to 16% and the  $\bar{\epsilon}_{eq,u}/\epsilon_u$  is 17%.

Although only few data were examined, it is observed that the length of the equivalent defect decreases by increasing the aggressiveness of the attack (thus the Scenarios), and that the reduction in the elongation capacity becomes remarkable in the case of localized attack (Scenario 2 and 3). The definition of an equivalent defect length (in which the minimum cross-section is modeled) related to the Scenarios may be a straightforward and effective strategy to carry out sensitivity analyses of the structural behavior, albeit more data are required from corroded bars, hence allowing the use of a probabilistic approach.

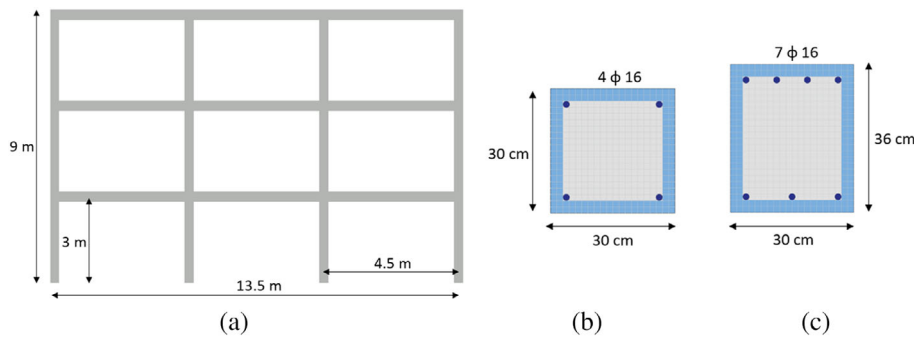


**FIGURE 5** Geometry and dimensions of the reference 2D frame (a) and characteristics of the column (b) and beam (c) cross-sections modeled through fiber elements

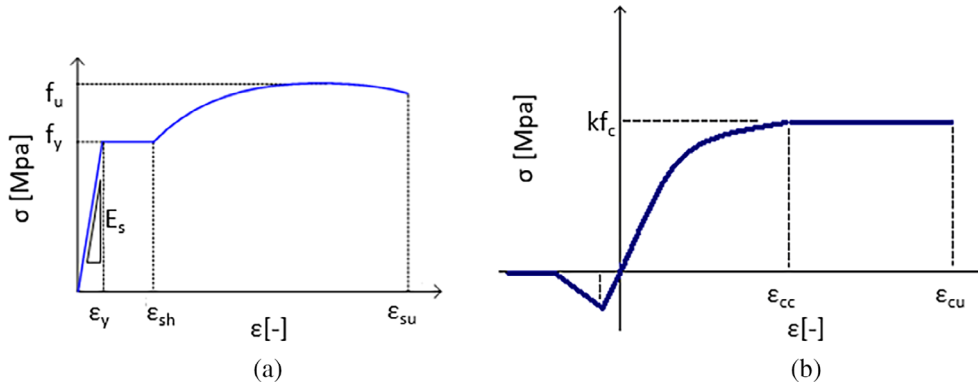


**FIGURE 6** Uniaxial stress-strain relationship used for inelastic material models: Park model for steel (a) and Nagoya highway corporation model for concrete (b)<sup>26</sup>

**TABLE 2** Corrosion attack characteristics selected for each scenario, with aggressiveness class H

CRS—Class	$T_p$ (years)	$v_{avg}$ ( $\mu\text{m}/\text{year}$ )	$R_p$	$L_c/L_{element}$
1-H	40	10	2	10%
2-H	40	30	5	5%
3-H	40	50	7	1.5%

### 3 | SEISMIC VULNERABILITY OF RC FRAMES FOR DIFFERENT CORROSION RISK SCENARIOS AND PATTERNS

In the following section, different corrosion patterns and Scenarios are simulated on a reference 2D RC frame, in order to show how the equivalent damage parameters calibrated in Section 2, according to the DEMSA protocol, can be implemented in structural engineering applications.

#### 3.1 | Description of the reference RC frame and modeling technique

The reference 2D 3-bay and 3-storey frame is shown in Figure 5a. A bay length  $L = 4.5$  and an inter-storey height  $H = 3$  m are assumed, for a total dimension of

$13.5 \times 9$  m. In the uncorroded condition, the columns have a cross-section of  $30 \text{ cm} \times 30 \text{ cm}$  and  $4\phi 16$  as reinforcement (Figure 5b), while the beams have a section of  $30 \text{ cm} \times 36 \text{ cm}$ , with  $4\phi 16$  and  $3\phi 16$  as top and bottom reinforcements, respectively (Figure 5c). The concrete cover depth is  $c = 3$  cm. A distributed load on the beams equal to  $32 \text{ kN/m}$  is considered to represent the dead floor load. Each structural element is divided into a number of nonlinear finite fiber elements (from 10 to 13 depending on the corrosion pattern) and the number of integration sections along the single element varies between 3 and 7 to have a homogeneous distance between them. The element section is divided in fiber cells (dimensions of concrete cells  $1.5 \text{ cm} \times 1.5 \text{ cm}$ ) as reported in Figure 5b,c. The models proposed in the following applications adopt force-based formulations and present a hardening sectional response, so the problem of localization does not affect the structural behavior<sup>29</sup>; discretization of the mesh and the number of integration sections were carefully calibrated to avoid mesh dependency issues.

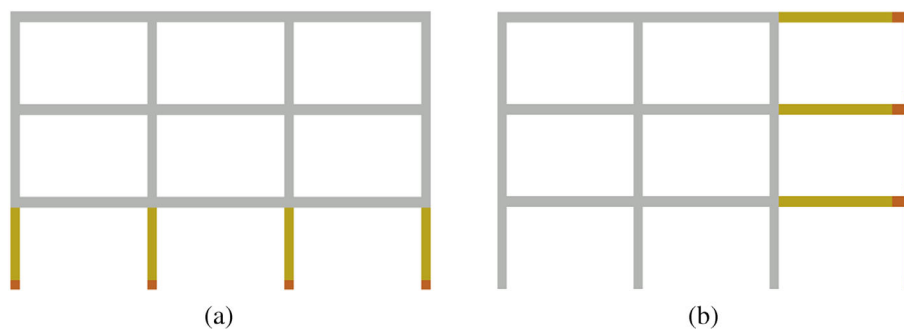
Fiber modeling technique is particularly suitable to describe the nonlinear behavior of RC structures<sup>23,24</sup>; it allows for the definition of several sections for the structural element, each one divided into a number of fiber cells, which can be characterized by different material properties. Through these models, the concrete cross-section geometry and mechanical properties, as well as the reinforcement detailing can thus be varied within the



**TABLE 3** Equivalent damage parameters in each scenario for corroded beams and columns compared with the original properties: average and minimum residual bar diameter, compressive strength of cracked concrete

CRS—class	$\phi_{\text{avg}}$ (mm)	$\phi_{\text{min}}$ (mm)	$f_c^*$ avg (MPa) column	$f_c^*$ avg (MPa) beam
No damage	16.0	16.0	25.0	25.0
1-H	15.6	15.2	13.6	10.2
2-H	14.8	10.0	7.1	4.7
3-H	14.0	2.0	4.8	3.1

**FIGURE 7** Two possible corrosion patterns on the reference RC frame: In P1, the columns at the ground floor are corroded (a), while in P2 the elements of the external bay (b)



same element. To date, fiber models are seldom adopted in professional practice, requiring time-consuming analyses and an accuracy in modeling the non-linear behavior of materials, which is usually out of the scope of structural assessment in the case of ordinary undamaged structures; however, they may be useful to investigate the structural behavior in the case of relevant nonlinearity which may govern the resistant mechanisms, due to, for example, corrosion damage. Simplified formulations, such as equivalent models to modify the constitutive relationship of plastic hinges<sup>25</sup> of corroded elements should then be developed and implemented in the lumped plasticity approach, starting from fiber model results.

The Park Model (with  $f_y = 360$  MPa,  $f_u = 540$  MPa,  $E_s = 210,000$  MPa,  $\epsilon_{sh} = 0.009$ ,  $\epsilon_{su} = 0.1$ ) and Nagoya Highway corporation Model (with  $f_c = 25$  MPa,  $\epsilon_{cc} = 0.002$ ,  $\epsilon_{cu} = 0.004$ ) are adopted as constitutive relationship for steel and concrete material, respectively<sup>26</sup> (see Figure 6 for the introduced symbols). The steel material properties defined for the initial uncorroded bar are kept constant, while for concrete, the cracked cover compressive strength is reduced, according to the average corrosion attack penetration (Section 2.1); possible beneficial confinement effect on the concrete core compressive strength is neglected (thus  $k = 1$ ).<sup>6</sup> It should be highlighted that, by reducing only the compressive strength and keeping the same limits of deformation for the concrete material, the stiffness of the cracked concrete cover is inherently reduced. Not complete agreement has been found in the literature yet; in other works<sup>27,28</sup> the peak and ultimate concrete strain values are reduced with the same factor used for strength, thus keeping the same stiffness. Doubts arise on which

strategy may be more representative of the actual behavior of cracked concrete, and further research is needed on this aspect.

In this analysis, the shear inelastic behavior is not modeled and failure is assumed to occur for flexure; also, the effects of reinforcement corrosion on bond interaction and possible buckling of longitudinal rebars are neglected in this preliminary phase, thus the hypothesis of the conservation of plane sections is adopted.

Therefore, the EDPs included in the FEM models to account for the effects of corrosion are the reduction of longitudinal bars cross-section (only the average and minimum residual cross-sections are modeled) and the reduced compressive strength of the concrete cover. Furthermore, the corrosion attack distribution along the element length is introduced through the simplified approach presented in Section 2.2.1 to also consider ductility reduction. In the corroded structural elements, two different types of sections are thus modeled: one with the minimum bar cross-section in a portion defined as the equivalent defect length ( $L_c$ ), and one with the average residual bar cross-section in the remaining element length ( $L_{\text{element}} - L_c$ ). This way the possible reduction of the bar elongation capacity due to plastic strain concentration in the defect is automatically computed since in fiber models, the actual stress and strain present in the fibers at sectional level is calculated at each step of the analysis. The length of the equivalent defect ( $L_c$ ) is chosen according to the preliminary considerations in Section 2.2.2 (Figure 4) in relation to Corrosion Risk Scenarios. The simplifications made allows defining a model, in which the variation of the structural response due to the introduction of both corrosion effects at a sectional level and the equivalent defect can be observed.

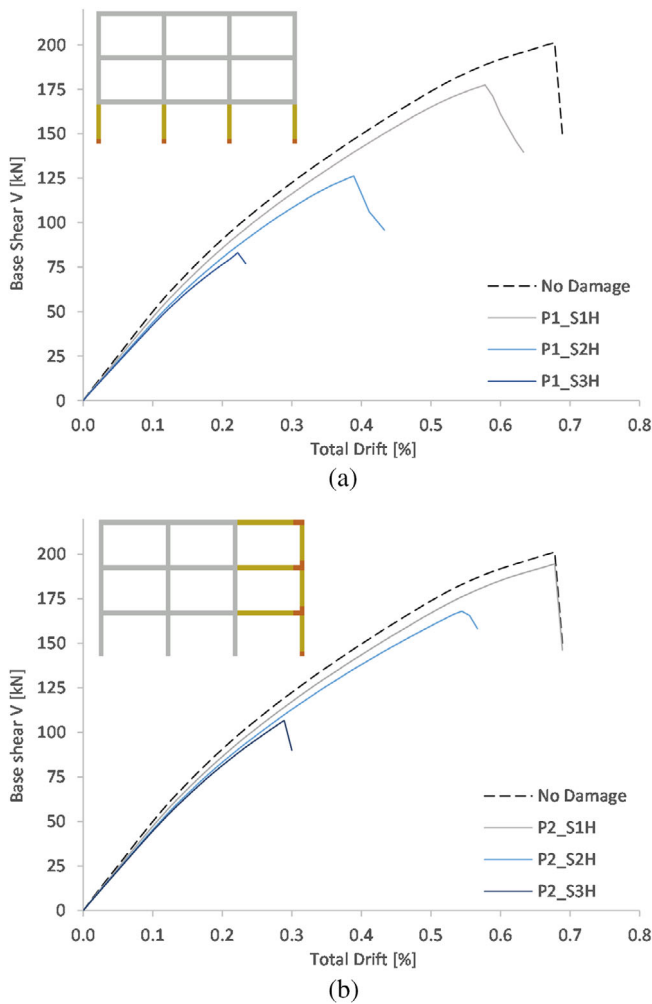


**FIGURE 8** Comparison of capacity curves of the reference frame in the undamaged condition (“no damage”), in corrosion risk scenario S1H, S2H, S3H for corrosion pattern P1 (a) and P2 (b)

**TABLE 4** Residual capacity in terms of base shear and total drift with respect to the “no damage” condition

CRS—class	Pattern P1		Pattern P2	
	$V/V_0$ (%)	$D/D_0$ (%)	$V/V_0$ (%)	$D/D_0$ (%)
1-H	88.2	85.2	96.8	100.0
2-H	62.7	57.4	83.5	80.3
3-H	41.3	32.8	53.0	42.6

### 3.2 | Description of the corrosion attack patterns and Scenarios

As for the definition of the equivalent damage parameters, Section 2, based on the DEMSA Protocol procedure, is followed. First, corrosion attack characteristics are defined: a representative value of the average corrosion rate  $v_{\text{avg}}$  and a maximum to average attack ratio  $R_p$  are selected from Table 1 for each Scenario (assuming an

aggressiveness class H), as reported in Table 2. For a better comparison of the possible corrosion effects on the structural behavior in different Scenarios, Model 2 (Figure 2) for the corrosion attack penetration on the bar section is chosen for all the Scenarios. Also, the initiation time is assumed as  $T_i = 10$  years, while the structure age is equal to  $T_a = 50$  years; thus, the propagation time results as  $T_p = 40$  years. Not enough data are available yet to associate the length of the equivalent defect (to model the maximum attack) with the Corrosion Risk Scenarios. As a proof of the concept, for a preliminary evaluation of the worst condition, the defect is modeled in correspondence of the expected location of plastic hinges in each element (at the columns base and at the beams end), and the defect length  $L_c/L_{\text{element}}$  is defined as a percentage of the element length. This may represent a portion of the expected plastic hinge length, and such a percentage decreases by increasing the aggressiveness of the attack (according to  $L_c/L_b$  reported in Figure 4b). It is worth noting that, according to Section 2.2, the role of the single defect is to represent a possible uneven distribution of the residual cross-section of the bar in natural conditions. Starting from the corrosion attack characteristics in Table 2, the average and minimum residual bar diameter ( $\phi_{\text{avg}}$  and  $\phi_{\text{min}}$ ) and the reduced compressive strength in the concrete cover  $f_c^*$  can be calculated from Equations 1–6 (Table 3).

When considering a whole structural system or sub-assembly, also the spatial variability of the attack among the structural elements is relevant. In the following, two examples are shown, by modeling two different corrosion patterns on the reference frame. In the first pattern P1 (Figure 7a), the columns at the ground floor are corroded, while all the other elements do not present corrosion damage; this may be the case of an external open colonnade where the columns are not sheltered from rain and the other elements present finishing. The second pattern P2 (Figure 7b) presents an external bay where the structural elements (both beams and columns) are more exposed to the environment. The portions represented in yellow and orange indicate the average and maximum corrosion attack, respectively. In the following section, capacity curves are derived for the corroded frames, by implementing the equivalent damage parameters calibrated for each Scenario in both the corrosion patterns; the curves are compared with the reference condition in absence of corrosion damage (“No Damage”).

### 3.3 | Capacity curves of the corroded RC frames

Capacity curves describing the base shear—total drift relation at 50 years of service life in the three different

**FIGURE 9** Example of 3D frame with corrosion pattern P2 modeled in the 2D frame in x-direction (a) and corrosion pattern P3 (b)

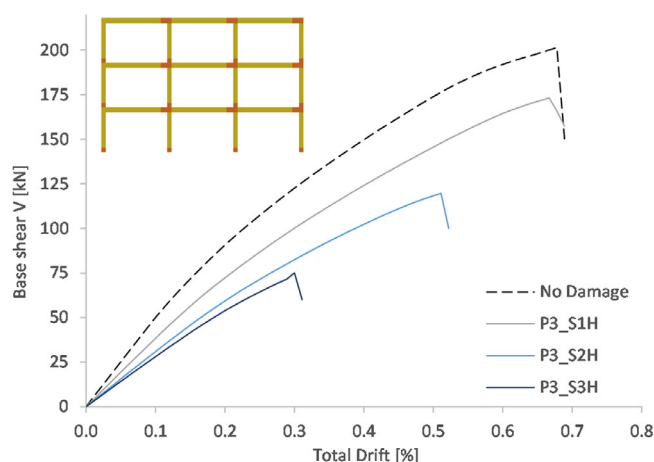
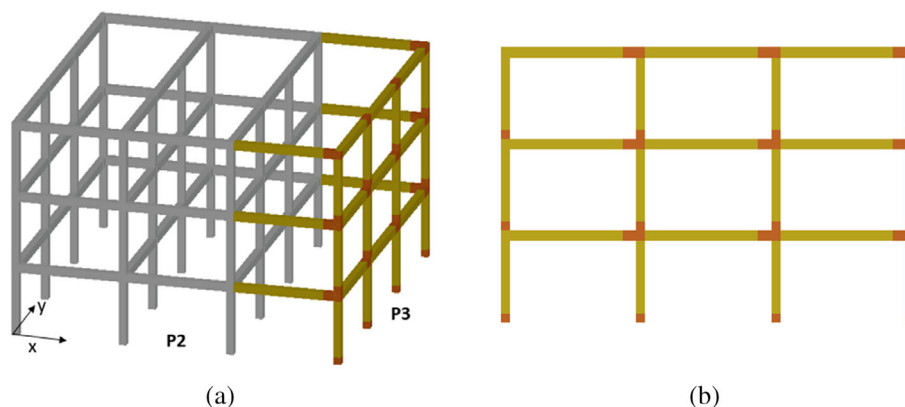


**FIGURE 10** Comparison of capacity curves of the reference frame in the undamaged condition (“no damage”), in corrosion risk scenario S1H, S2H, S3H for corrosion pattern P3

Scenarios are obtained through nonlinear static analysis with the software MidasGen.<sup>26</sup> Results are reported in Figure 8a,b and Table 4 for corrosion pattern P1 and P2, respectively. A slight global elastic lateral stiffness reduction is observed for the corroded frames, due to the lower compressive strength of the concrete cover in the damaged condition. Since the reference frame, in the undamaged condition, is mainly dominated by a soft-storey collapse mechanisms at the ground floor, the corrosion of the columns at the base strongly affects the structural response both in terms of shear capacity and ductility. Pattern P1 is thus most critical than pattern P2 for the considered frame. However, in both cases, corrosion leads to lower structural performances with respect to the uncorroded condition. Since the capacity in terms of base shear is governed by the characteristics of the column base section, while the displacement capacity is related to the maximum attack length and the difference between the minimum and average residual cross-section along the bar length, capacity reduction increases by varying the Corrosion Risk Scenario from 1 to 3. Indeed, the

length of the defect with the maximum attack decreases from Scenario 1 to 3, and the difference between the average and minimum bar residual cross-section increases.

In all the analyses, failure occurs due to concrete crushing in the section at the columns base, even when a very low residual reinforcement ratio is observed. Indeed, with the maximum strain of the concrete material set equal to 0.4% and having adopted the hypothesis of conservation of plane sections, plastic strain in the steel at failure is always much smaller than the ultimate strain, which is set as equal to 10%.

### 3.4 | Further considerations on the structural behavior and residual life

The analyses carried out on 2D frames emphasizes the importance of implementing equivalent damage parameters in the structural assessment since both the single structural element capacity and the global behavior may be strongly affected by corrosion damage. The irregular spatial variability of the corrosion attack leads to further consequences on the structural behavior when considering a 3D building subjected to deterioration. As a proof of the concept, a 3D frame is considered, composed by two reference 2D frames in the x-direction and four frames in the y-direction (Figure 9a). The outer frames in the x-direction are supposed to present the corrosion pattern P2; while the right-side frame in the y-direction is characterized by the corrosion pattern P3 (Figure 9b), with a corrosion damage affecting all the structural elements, representing, for example, a situation where all the structural elements are exposed to the environment without finishing.

The capacity curves of the reference frame with corrosion pattern P3 are reported for all the Scenarios in Figure 10. It is observed that, for the same external load (i.e., for the same base shear), a remarkable reduction of

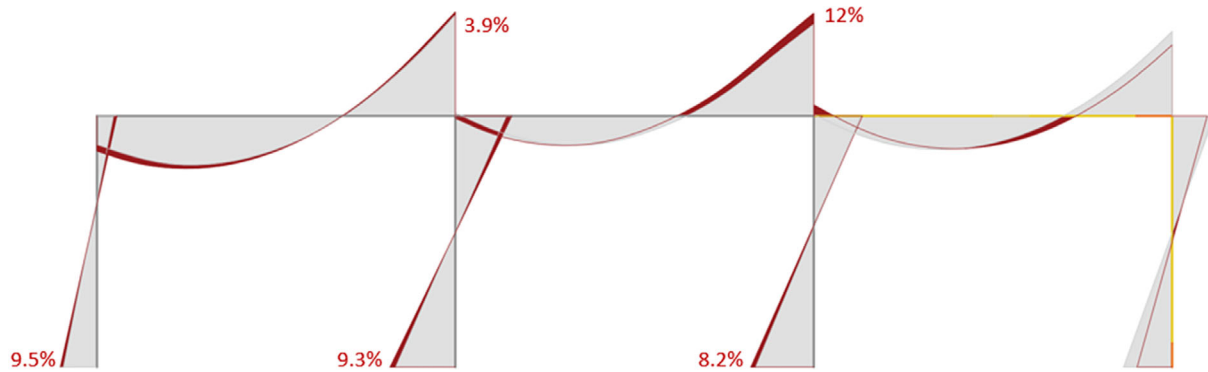


**FIGURE 11** Bending moment internal distribution in case of “no damage” condition (gray diagram) and in the case of corrosion pattern P2\_S2H at 50 years (red diagram). The red solid fill indicates the increase of internal bending moment. Only the ground floor is reported for sake of clarity

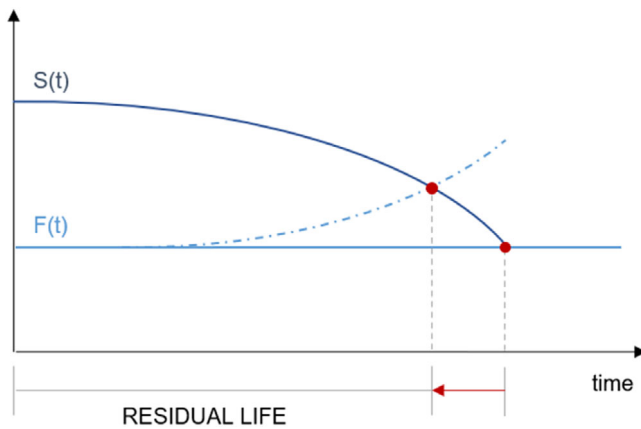


**FIGURE 12** Qualitative example of simultaneous element capacity  $S(t)$  reduction and internal force  $F(t)$  increase in time, leading to a further reduction of the residual life with respect to keeping constant the internal force distribution

the elastic stiffness is observed in case of corroded frames with respect to the uncorroded one, together with a reduction of the ductility.

In this case, considering the building subjected to horizontal loads, different behaviors may be expected in the  $x$ -direction and in the  $y$ -direction. In the  $x$ -direction, the two frames present the same corrosion pattern, so a behavior similar to the ones of the 2D single frame may be expected. On the other hand, in the  $y$ -direction, only the outer frame presents the P3 corrosion pattern; as a consequence, significant relative horizontal displacements may occur between the outer frame and the other non-corroded frames, leading to a redistribution of the forces among the frames and to additional shear forces in the floor diaphragm. Such forces may compromise the integrity of the diaphragm also for an external load lower than the building capacity.

Also, a variation in element stiffness can cause a redistribution of internal actions in the structure, and this effect is more relevant in cases when some portions of the structure remain integer or are subjected to a less aggressive attack. In those sections, indeed, an increase in the internal actions with respect to the undamaged condition may be observed, both for static and seismic loads. Figure 11 reports the comparison of the bending moment distribution at the ground floor of the reference 2D frame in the “No Damage” condition (internal actions in gray) and in case of corrosion pattern P2 and Scenario S2H (internal actions in red) for an external seismic load of 150 kN (pushover curves in Figure 8b, corresponding to a total drift of 0.37% and 0.45% mm for “No Damage” and “P2\_S2H”, respectively); the beam and column on the right are modeled with the average (yellow) and maximum (orange) corrosion attack described in Table 3 (S2H, 50 years), according to pattern P2.

It is observed that, while in the corroded areas the internal bending moment decreases due to the lower stiffness and maximum capacity of the structural elements, in the adjacent areas the maximum bending moment increases (red solid fill in Figure 11), with a maximum value of 12% with respect to the “No Damage” condition at the right end of the central beam and a value ranging between 8% and 10% at the columns base. This example stems as a proof of the concept that critical conditions may be found in some areas which are not believed to be critical in the undamaged state. Moreover, if the undamaged areas were also corroded, but with a lower intensity attack, an increase in the internal action may occur simultaneously with a reduction of strength. The obtained results outline the importance of evaluating not only the single structural element deterioration, but also its effect on the whole structural system. Indeed, while the capacity of the elements decreases in time according

to the deterioration level, an increase in internal actions in the elements themselves may occur, with a further reduction of the building structural residual life (Figure 12).

## 4 | CONCLUDING REMARKS AND RESEARCH OUTLOOKS

Simple equivalent damage parameters (EDP) enabling the modeling of expected corrosion damage in the structural assessment have been introduced. These parameters are calibrated by adopting formulations available in the literature, starting from easy-measurable environmental and aggressiveness conditions. Although more data on naturally corroded bars are required to perform a more comprehensive and accurate characterization of the corrosion attack in each Corrosion Risk Scenarios, and complete agreement on the modified constitutive relationship of deteriorated material has not been found yet, the engineering applications presented in this paper show the effectiveness of these parameters in identifying possible corrosion effects on the structural performances.

Since the spatial variability of the corrosion attack within the single structural element may determine a reduction in the element ductility, a simplified approach based on the definition of a single equivalent defect where the maximum attack is present is also introduced in this paper, and it can be used for preliminary evaluations; also in this case, further research is needed to establish a correlation between natural corrosion patterns and the length of such a single defect. This topic is subject of ongoing research.

Nonlinear static analyses on a reference 2D frames carried out in this paper show that the impact of possible corrosion effects cannot be disregarded, addressing both the evaluation of the as-is condition of a deteriorated structure, its future service life, and the choice of the best renovation strategy. Beside the direct consequences of corrosion phenomena, it was demonstrated that the interaction of corroded elements in the structural sub-assembly may lead to a redistribution of the internal actions, thus changing the configuration of critical zones within the structure, and possibly further reducing the building structural residual life. The spatial variability of the corrosion attack in real buildings may lead to further consequences on other structural or non-structural elements, such as for example the increase of the shear action in the floor diaphragm due to high relative displacements between adjacent frames.

In a future development of this work, more investigations about corrosion effects on structural behavior of RC buildings should be carried out to further improve the representativeness of the proposed EDPs. In addition, other aspects such as shear inelastic behavior and steel-concrete bond interaction, among others, may be integrated in the nonlinear models to investigate also their impact on the structural performances. Finally, results of fiber models may be used to derive simplified formulations of plastic hinges to be included in more straightforward lumped plasticity approach.

## DATA AVAILABILITY STATEMENT

Data sharing is not applicable to this article as no new data were created or analyzed in this study.

## ORCID

Elena Casprini  <https://orcid.org/0000-0003-2244-8212>

Chiara Passoni  <https://orcid.org/0000-0002-6370-8992>

Alessandra Marini  <https://orcid.org/0000-0002-1798-2966>

Gianni Bartoli  <https://orcid.org/0000-0002-5536-3269>

## REFERENCES

- Bertolini L, Elsener B, Pedferri P, Redaelli E, Polder R. Corrosion of steel in concrete - prevention, diagnosis, repair. Weinheim: Wiley VCH; 2013.
- Andrade C. Propagation of reinforcement corrosion: principles, testing and modelling. *Materials and Structures*. 2019;52(2): 1-26. <https://doi.org/10.1617/s11527-018-1301-1>
- Coronelli D. Resistance of corroded RC beams: Extending fib Model Code 2010 models. *Structural Concrete*. 2010;2020:1-16. <https://doi.org/10.1002/suco.201900311>
- Proceedings of the fib CACRCS DAYS 2020 - Capacity assessment of Corroded Reinforced Concrete Structures*. Edited by: Beatrice Belletti, Dario Coronelli. ISBN 978-2-940643-10-3.
- Abstract Proceedings of the fib CACRCS DAYS 2021 - Capacity assessment of Corroded Reinforced Concrete Structures from Research to Daily Engineering Evaluation*. Edited by: Beatrice Belletti, Dario Coronelli. ISBN 978-2-940643-14-1.
- Casprini E, Passoni C, Marini A, Bartoli G. DEMSA protocol: deterioration effects modelling for structural assessment of RC buildings. *Buildings*. 2022;12(5):574.
- Zhu W, François R. Structural performance of RC beams in relation with the corroded period in chloride environment. *Materials and Structures*. 2015;48:1757-69. <https://doi.org/10.1617/s11527-014-0270-2>
- Casprini E. A protocol for the assessment of corrosion effects in RC structures in a life cycle engineering framework. PhD Dissertation. Bergamo: University of Bergamo, Department of Engineering and Applied Sciences; 2021.
- CONTECVET IN30902I. A validated user manual for assessing the residual life of concrete structures. DG Enterprise, CEC; 2001.



- Available online: <https://www.ietcc.csic.es/en/> (accessed on 26 April 2022).
10. EN 206:2013. Concrete-specification, performance, production and conformity.
  11. Çağatay HI. Experimental evaluation of buildings damaged in recent earthquakes in Turkey. *Eng Fail Anal.* 2005;12:440–52.
  12. Martínez I, Andrade C. Examples of reinforcement corrosion monitoring by embedded sensors in concrete structures. *Cem Concr Compos.* 2009;31:545–54.
  13. RILEM. Durability design of concrete structures. London: E&FN Spon; 1996; Report no. 14.
  14. Tuutti K. Corrosion of steel in concrete. Stockholm: Swedish Cement and Concrete Research Institute; 1982.
  15. Andrade C. Approach to the residual strength of steel bars due to corrosion. *Proceedings of the fib CACRCS DAYS*; 2021:13–17.
  16. Palsson R, Mirza MS. Mechanical response of corroded steel reinforcement of abandoned concrete bridge. *ACI Struct J.* 2002; 99:157–162.
  17. Imperatore S, Rinaldi Z, Drago C. Degradation relationship for the mechanical properties of corroded steel rebars. *Constr Build Mater.* 2017;148:219–30.
  18. Walrawen J. Significance of reinforcement corrosion for modelling the behaviour of existing concrete structures. *Proceedings of the fib CACRCS days*; 2020.
  19. Coronelli D, Gambarova PG. Structural assessment of corroding R/C beams: modelling guidelines. *ASCE J Struct Eng.* 2004; 130(8):1214–24.
  20. Molina FJ, Alonso C, Andrade C. Cover cracking as a function of rebar corrosion. II: numerical model. *Mater Struct.* 1993;26:532–48.
  21. Chen E, Berrocal CG, Fernandez I, Lofgren I, Lundgren K. Assessment of the mechanical behaviour of reinforcement bars with localised pitting corrosion by digital image correlation. *Eng Struct.* 2020;219:110939.
  22. Casprini E, Passoni C, MA Bartoli, Modelling corrosion effects in reinforced concrete structural members through equivalent damage parameters. *Proceedings of the Fib CACRCS days*; 2021: 127–130.
  23. Spacone E, Filippou F, Taucer FF. Fibre beam-column model for non-linear analysis of R/C frames: Part I. Formulation. *Earthq Eng Str Dyn.* 1996;25(7):711–26.
  24. Dizaj EA, Madandoust R, Kashani MM. Probabilistic seismic vulnerability analysis of corroded reinforced concrete frames including spatial variability of pitting corrosion. *Soil Dyn Earthq Eng.* 2018;114:97–112.
  25. Berto L, Vitaliani R, Saetta A, Simioni P. Seismic assessment of existing RC structures affected by degradation phenomena. *Struct Saf.* 2009;31:284–97.
  26. MidasGEN. User Manual, release 2020.
  27. De domenico D, Messina D, Recupero A. Cyclic behavior prediction of corroded reinforced concrete columns through a fiber hinge model. *Proceedings of the fib CACRCS DAYS*; 2021: 101–104.
  28. Franceschini L, Vecchi F, Belletti B. The PARC\_CL 2.1 crack model for NLFEA of reinforced concrete elements subjected to corrosion deterioration. *Corros Mater Degrad.* 2021;2:474–92. <https://doi.org/10.3390/cmd2030025>
  29. Coleman J, Spacone E. Localization issues in force-based frame elements. *J Struct Eng.* 2001;127(11):1257–65.

## AUTHOR BIOGRAPHIES



**Elena Casprini**, Post-doc researcher, Department of Engineering and Applied Sciences, University of Bergamo, 24044 Dalmine, Italy. Email: [elena.casprini@unibg.it](mailto:elena.casprini@unibg.it)



**Chiara Passoni**, Assistant professor, Department of Engineering and Applied Sciences, University of Bergamo, 24044 Dalmine, Italy. Email: [chiara.passoni@unibg.it](mailto:chiara.passoni@unibg.it)



**Alessandra Marini**, Full professor, Department of Engineering and Applied Sciences, University of Bergamo, 24044 Dalmine, Italy. Email: [alessandra.marini@unibg.it](mailto:alessandra.marini@unibg.it)



**Gianni Bartoli**, Full professor, Department of Civil and Environmental Engineering, University of Firenze, 50139 Firenze, Italy. Email: [gianni.bartoli@unifi.it](mailto:gianni.bartoli@unifi.it)

**How to cite this article:** Casprini E, Passoni C, Marini A, Bartoli G. Toward the definition of equivalent damage parameters for the assessment of corroded RC structures. *Structural Concrete.* 2022. <https://doi.org/10.1002/suco.202200368>